NUB 2269

ψ(3.1) PRODUCTION BY PIONS AND PROTONS AT FERMILAB*

9/15/75

CONF-75-196E
E-0365
C75/07/21

G. L. Blanar, C. F. Boyer, W. L. Faissler, D. A. Garelick†, M. W. Gettner, M. J. Glaubman, J. R. Johnson, H. Johnstad, M. L. Mallary, E. L. Pothier, D. M. Potter, M. T. Ronan, M. F. Tautz, E. von Goeler and Roy Weinstein

Presented‡ by M. T. Ronan

Northeastern University at Boston
Boston, Massachusetts 02115

#365

I will describe measurements of ψ(3.1)[1] meson production by pions and protons made by the Northeastern High Energy group at Fermi National Accelerator Lab, FNAL. I will give ψ production probabilities per inelastic collision, distributions in $X_L = P_{Lab}/P_{beam}$ and $P_\perp$, and the ratio of ψ yield per incident pion to that for protons as measured in the reactions

$$\pi^- + Fe \rightarrow \mu^+ + \mu^- + X \text{ at } P_{beam} = 200 \text{ GeV}$$

$$p + Fe \rightarrow \mu^+ + \mu^- + X \text{ at } P_{beam} = 240 \text{ GeV}$$

I will mention some features of the low mass region of our data. The di-muon data were taken during an experiment by our group which searched for charmed meson production in $\pi^- p$ and pp interactions. I will not describe the charm search experiment at this time.

The experiment[2] was performed in the M2 beam line in the Meson Lab at FNAL. The M2 beam is nominally a diffractive proton beam since it views the meson area target at a production angle of 1.0 m rad; however, by reversing the polarity of the bending magnets, an intense π^- beam can be obtained at slightly lower energies. Beam hodoscopes were used to measure the incident beam particle's momentum to $\delta p_B/p_B \sim 0.2\%$, and its incident vertical and horizontal angles to $\delta\theta \sim 0.2$ m rad. The beam spot at the target was 1/4" x 1/4" and the

---

* Research supported in part by the National Science Foundation under grant MPS70-02059A5.

† Sloan Foundation Fellow.

‡ Invited paper at the 1975 SLAC Summer Institute on Particle Physics.

coordinates of the beam particle were measured to an accuracy of 1/16" horizontally and 1/8" vertically. Beam particle identification was accomplished using two threshold Cerenkov counters set on pions. The beam part of the trigger included signals from beam trigger counters and the absence of signals from halo veto counters. One of the beam counters was pulse height analyzed.

The data I will present was taken in a total of 45 hours of beam time. A 200 GeV negative pion (less than 1% kaon) beam was used for 25 hours at an intensity of $\sim 6.0 \times 10^5$ per $\sim .8$ sec pulse. For the remaining time we used a 240 GeV proton (less than .5% pion) beam at $\sim 7.5 \times 10^5$/pulse.

The apparatus used for the di-muon experiment was a solid iron μ spectrometer shown in Fig. 1. The μ-pairs were created at the front end of the first iron (Fe) absorber. Muons were identified by their traversal of 5.6 m of iron. A 60 cm hydrogen target, not shown, used for the charm search experiment was centered $\sim$ 60 cm upstream of the iron. The MP counters were used to determine the effect of upstream interactions. Counters M0 thru M5 were the di-muon trigger counters. The first $\sim$ 2.5 m of iron served as both target and hadron absorber. A 3 m long gapless iron magnet, assembled and wound by us, was used in conjunction with 3 magnetostrictive spark chambers to measure muon production angles and momenta. The proportional chamber was used only in checking the reconstruction technique and the spark chamber efficiencies for a subsample of the data.

The di-muon trigger required a six fold counter concidence, $M0 \cdot M1 \cdot (M2 \cdot M3) \cdot (M4 \cdot M5)$ in time with a beam particle trigger. The following steps were taken to insure that at least two muons passed through the apparatus: pulse heights 1 1/2 times minimum ionizing were required for M0 and M1 and a split counter coincidence,

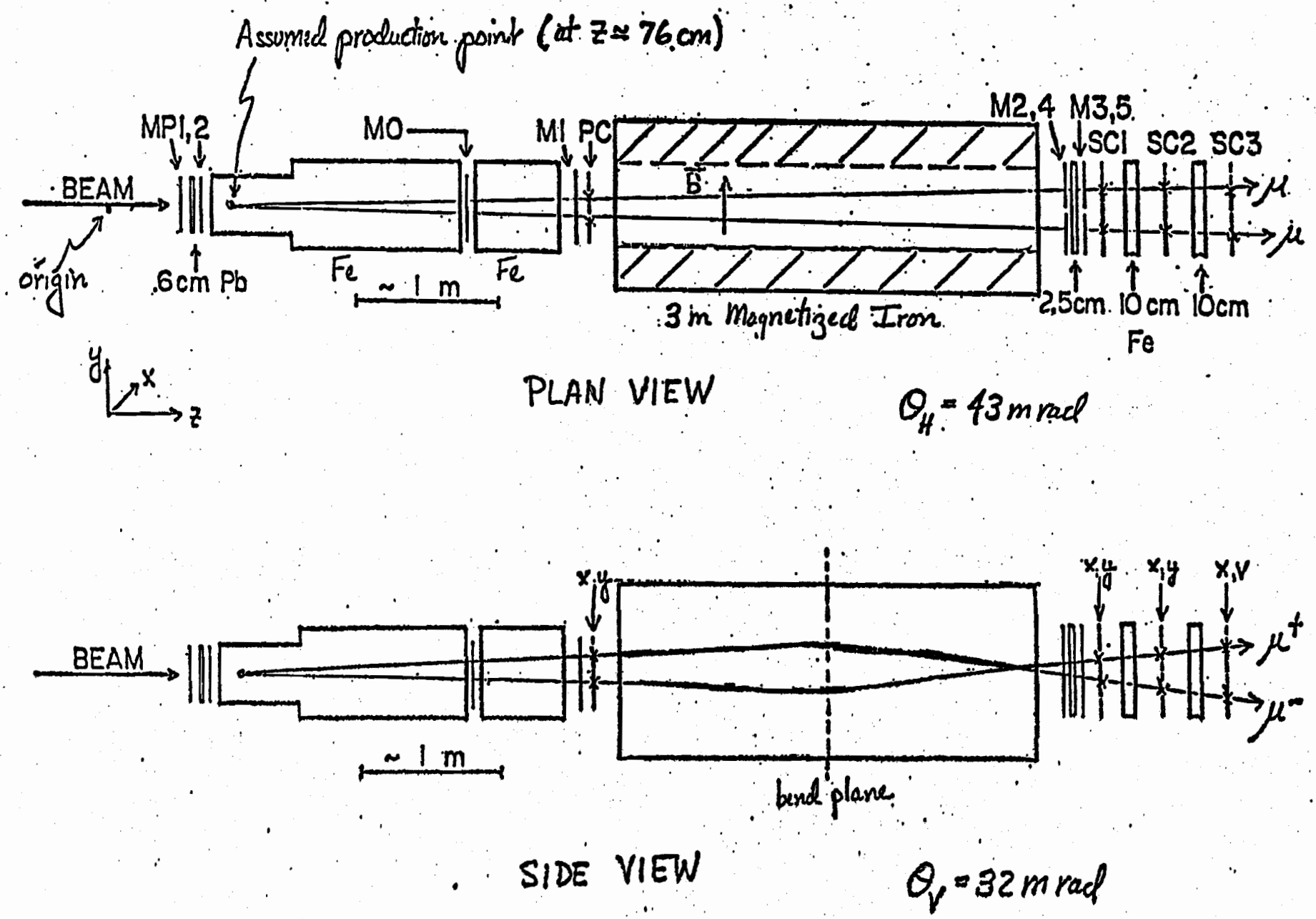
Assumed production point (at z ≈ 76 cm)
MP1,2
MO
M1
PC
M2,4
M3,5
SC1
SC2
SC3
BEAM
origin
.6 cm Pb
Fe
~ 1 m
Fe
B
3 m Magnetized Iron
2.5 cm
10 cm
10 cm
Fe
μ
μ
y
x
z
PLAN VIEW
θ_H = 43 m rad
x,y
x,y
x,y
x,V
BEAM
~ 1 m
bend plane
μ^+
μ^-
SIDE VIEW
θ_V = 32 m rad

Fig. 1

(M2·M3)·(M4·M5), was required at the rear of the magnet. Furthermore, iron was placed between the back trigger counters and between the spark chambers to eliminate backgrounds due to single muons which caused knock-on electrons. During the actual running we checked that there was no observable accidental component in the trigger. Also, we checked that the biases on the M0 and M1 counters were set well below the double minimum ionizing peak.

Alignments and magnet calibration were done using a μ beam. The M2 line is a two stage magnet system. In order to produce a μ beam, two collimators after the first stage were closed and the second stage was used to center the μ beam on a hodoscope just in front of the target. The momentum spectrum used to calibrate the iron magnet with 200 GeV muons is shown in Fig. 2. Superimposed are points obtained with a Monte Carlo program which simulates events in a model of our apparatus. The agreement is quite good. The calibration was checked at other values of the muon momentum. The magnetic field of the iron magnet was found in this way to be 18.5 Kilogauss. We have also found from an analysis of our wide opening angle events that the variation in average field over the active region of the magnet is less than 5%.

A study of the number of di-muon events, corrected for detection efficiency, per incident flux for a sample of the data runs checked the stability of the detector for the duration of the experiment.

The dimuon invariant mass, $M_{\mu\mu}$, was calculated from the tracks measured by the spark chambers, assuming the dimuon was produced inside the first iron absorber one absorption length from its edge along the beam line, at the point z = 76 cm in our coordinate system, see Fig. 1. The muon momenta and angles were reconstructed taking into account the bending and energy loss of the muons in the

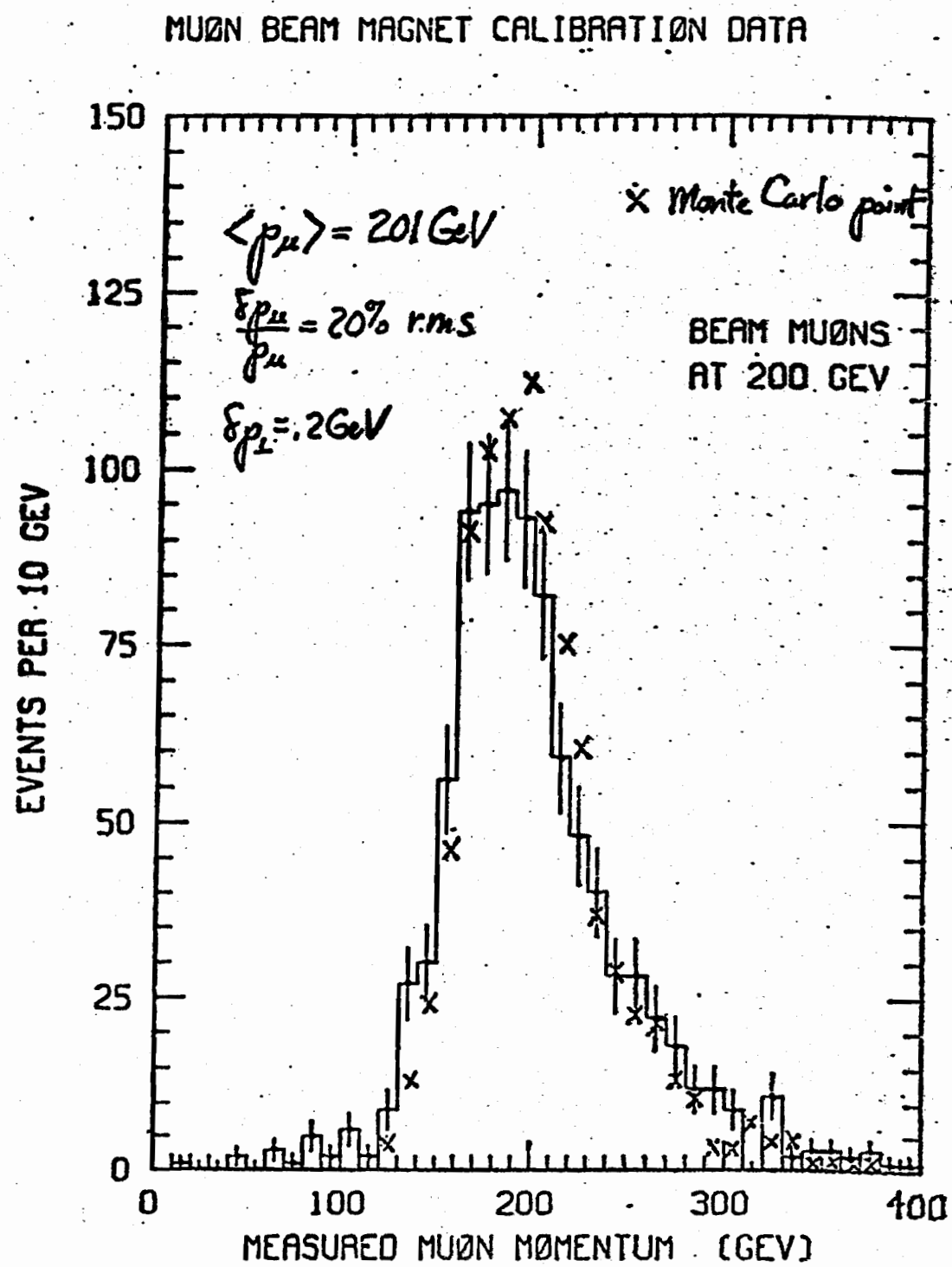
MUØN BEAM MAGNET CALIBRATIØN DATA
× Monte Carlo point
$\langle p_\mu \rangle = 201$ GeV
$\frac{\delta p_\mu}{p_\mu} = 20\%$ r.m.s
$\delta p_\perp = .2$ GeV
BEAM MUØNS
AT 200 GEV
EVENTS PER 10 GEV
150
125
100
75
50
25
0
0
100
200
300
400
MEASURED MUØN MØMENTUM (GEV)

Fig. 2

magnetized iron spectrometer.

Only $\mu^+\mu^-$ events were selected, eliminating $\approx$ 2% of the 2μ events. In the horizontal plane, where there is no bending, each muon track was extrapolated back to the assumed production point. The distribution of measured deviation at the production point divided by the expected standard deviation, calculated using the measured momentum of the track, was compared to a gaussian distribution, see Figs. 3 and 4. The discrepancy between the slope of .42 in Fig. 3 and the .5 one would expect for a gaussian distribution indicates an 8% error in our calculation of the expected standard deviation which is probably due to the fact that we neglected large angle Coulomb scattering. In the analysis, the tracks were required to deviate by less than 2.2 standard deviations removing $\approx$ 10% of the events. Note that we have placed the cut at a point near where the distribution for the pion beam data, Fig. 3, begins to deviate from the gaussian distribution; this deviation is peculiar to the pion beam data and we believe that it is due to a beam muon background.

For all of the data I will present we have required that the lab momentum of the di-muon be greater than 90 GeV; this insures that our acceptance for the events in the 3 GeV mass region is greater than $\sim$ 15%. For a fixed mass the acceptance of the apparatus is a smooth function of lab momentum, P_L, and transverse momentum, $P_\perp$. In the interval $2 \leq M_{\mu\mu} \leq 4$ GeV, the mass acceptance is a smooth structureless function of mass and varies by about $\pm$ 35%.

The dimuon effective mass spectra for the high mass region as observed are shown in Figs. 5 and 6. The dashed curves drawn in the region $M_{\mu\mu} \approx 3$ GeV represent the spectra calculated by a Monte Carlo method which takes into account the resolution and detection efficiency of the apparatus and assumes all of the events in the interval

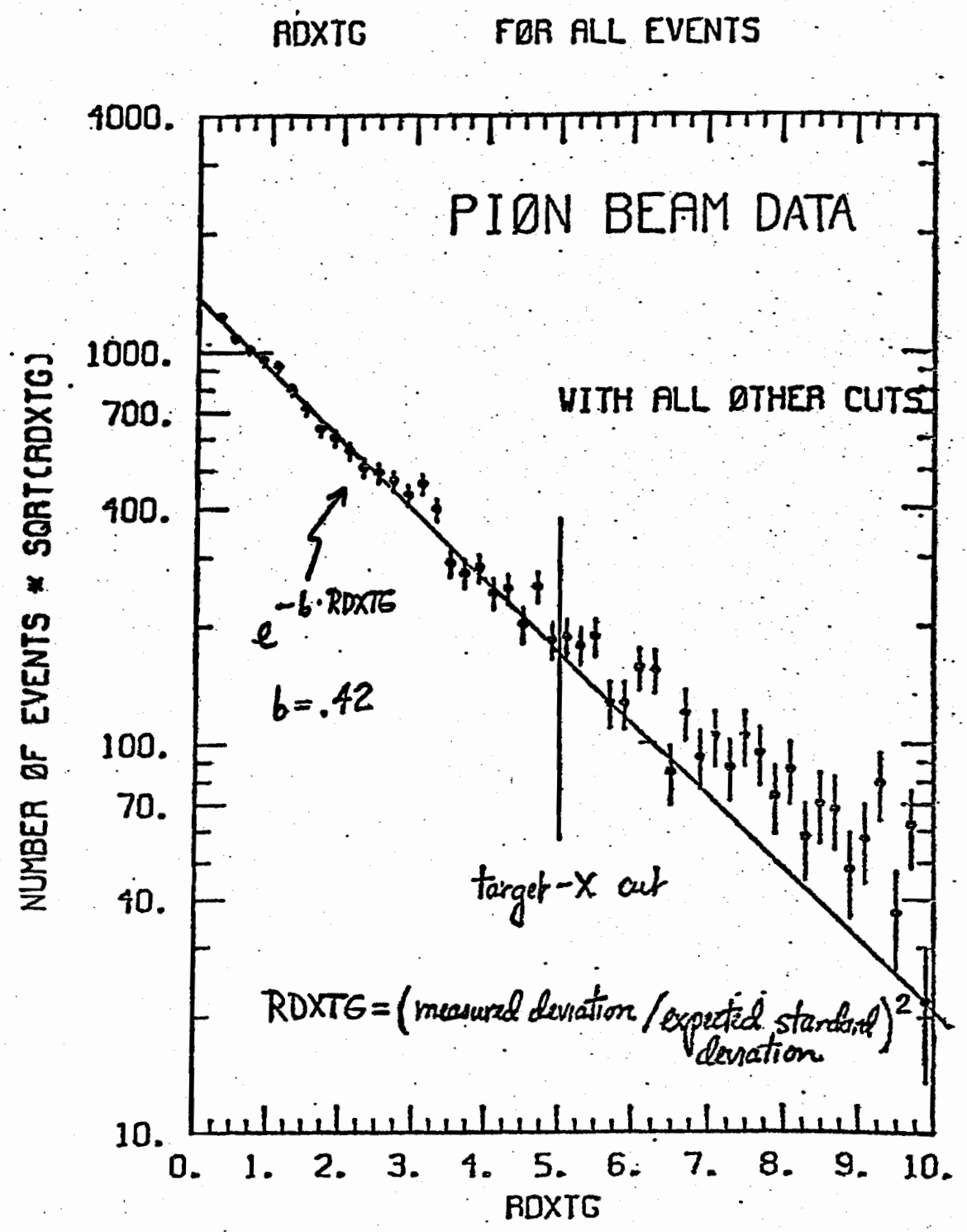
RDXTG FØR ALL EVENTS
PIØN BEAM DATA
WITH ALL ØTHER CUTS
NUMBER ØF EVENTS * SQRT(RDXTG)
1000.
700.
400.
100.
70.
40.
10.
0. 1. 2. 3. 4. 5. 6. 7. 8. 9. 10.
RDXTG
e^-b·RDXTG
b=.42
target-X cut
RDXTG=(measured deviation / expected standard deviation)^2

Fig. 3

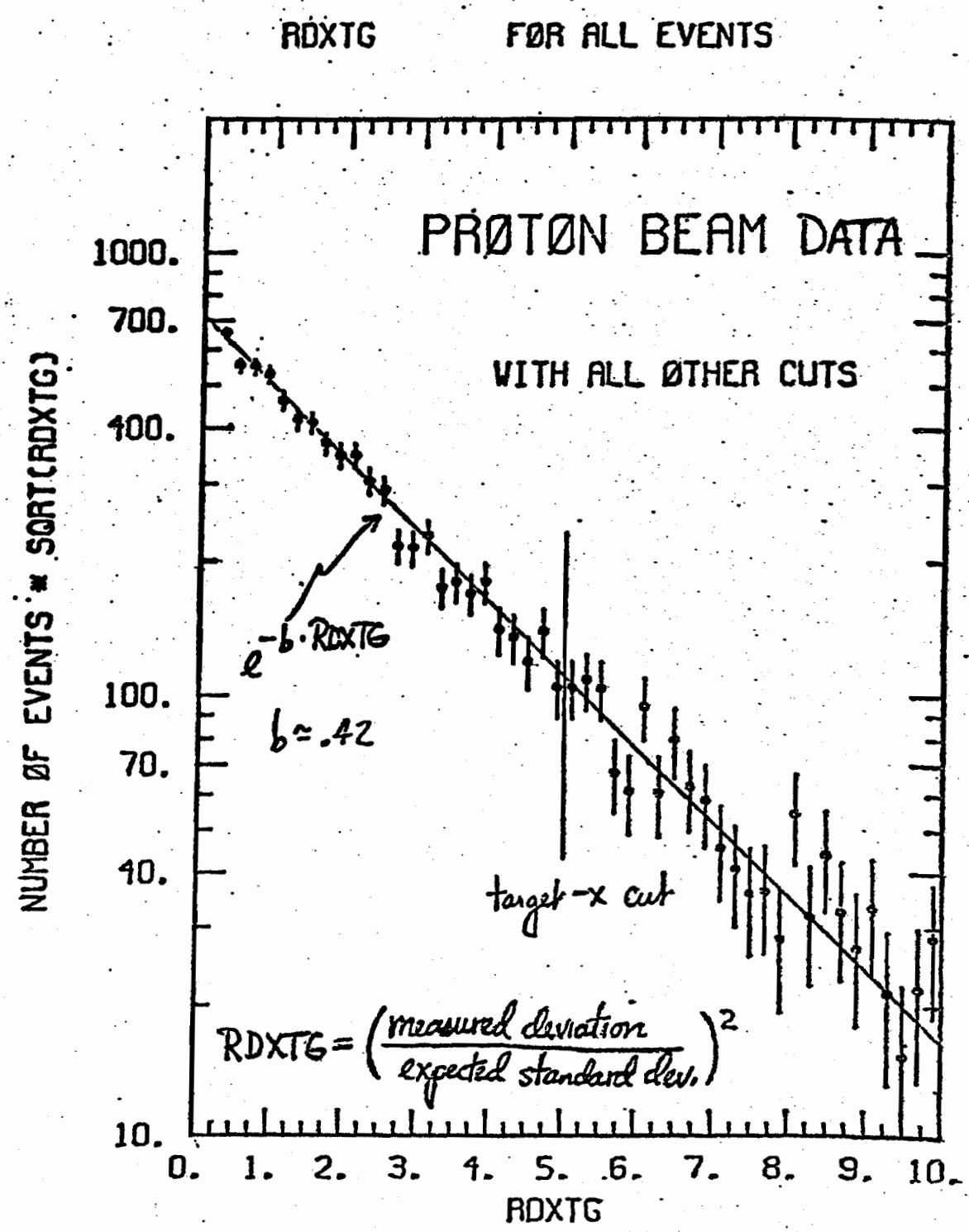
RDXTG FØR ALL EVENTS
PRØTØN BEAM DATA
WITH ALL ØTHER CUTS
NUMBER ØF EVENTS * SQRT(RDXTG)
1000.
700.
400.
100.
70.
40.
10.
0. 1. 2. 3. 4. 5. 6. 7. 8. 9. 10.
RDXTG
$e^{-b \cdot RDXTG}$
$b \simeq .42$
target-x cut
$RDXTG = \left(\frac{\text{measured deviation}}{\text{expected standard dev.}}\right)^2$

Fig. 4

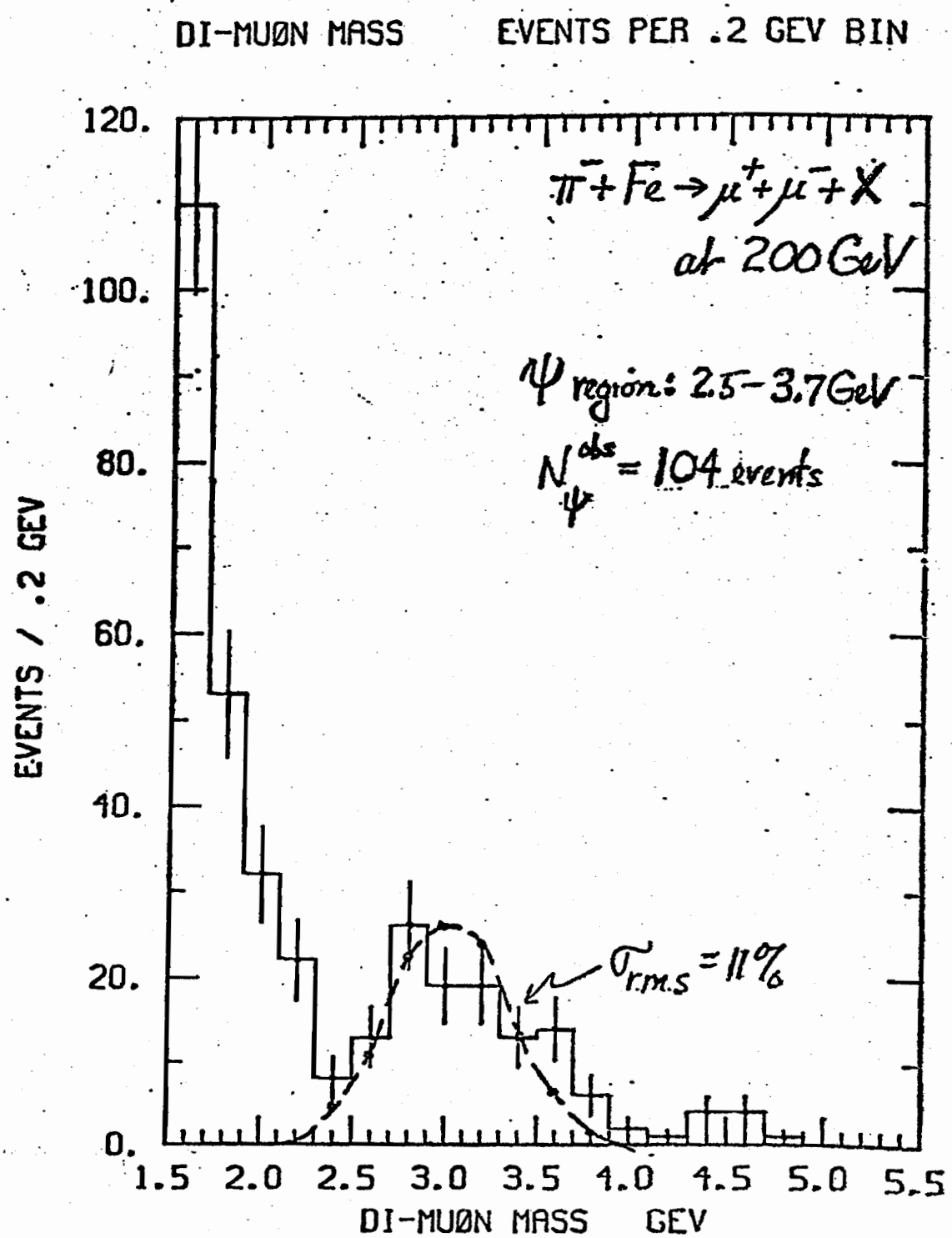
DI-MUØN MASS EVENTS PER .2 GEV BIN
$\pi^- + Fe \rightarrow \mu^+ + \mu^- + X$
at 200 GeV
ψ region: 2.5–3.7 GeV
$N_\psi^{obs} = 104$ events
$\sigma_{r.m.s} = 11\%$
EVENTS / .2 GEV
120.
100.
80.
60.
40.
20.
0.
1.5 2.0 2.5 3.0 3.5 4.0 4.5 5.0 5.5
DI-MUØN MASS GEV

Fig. 5

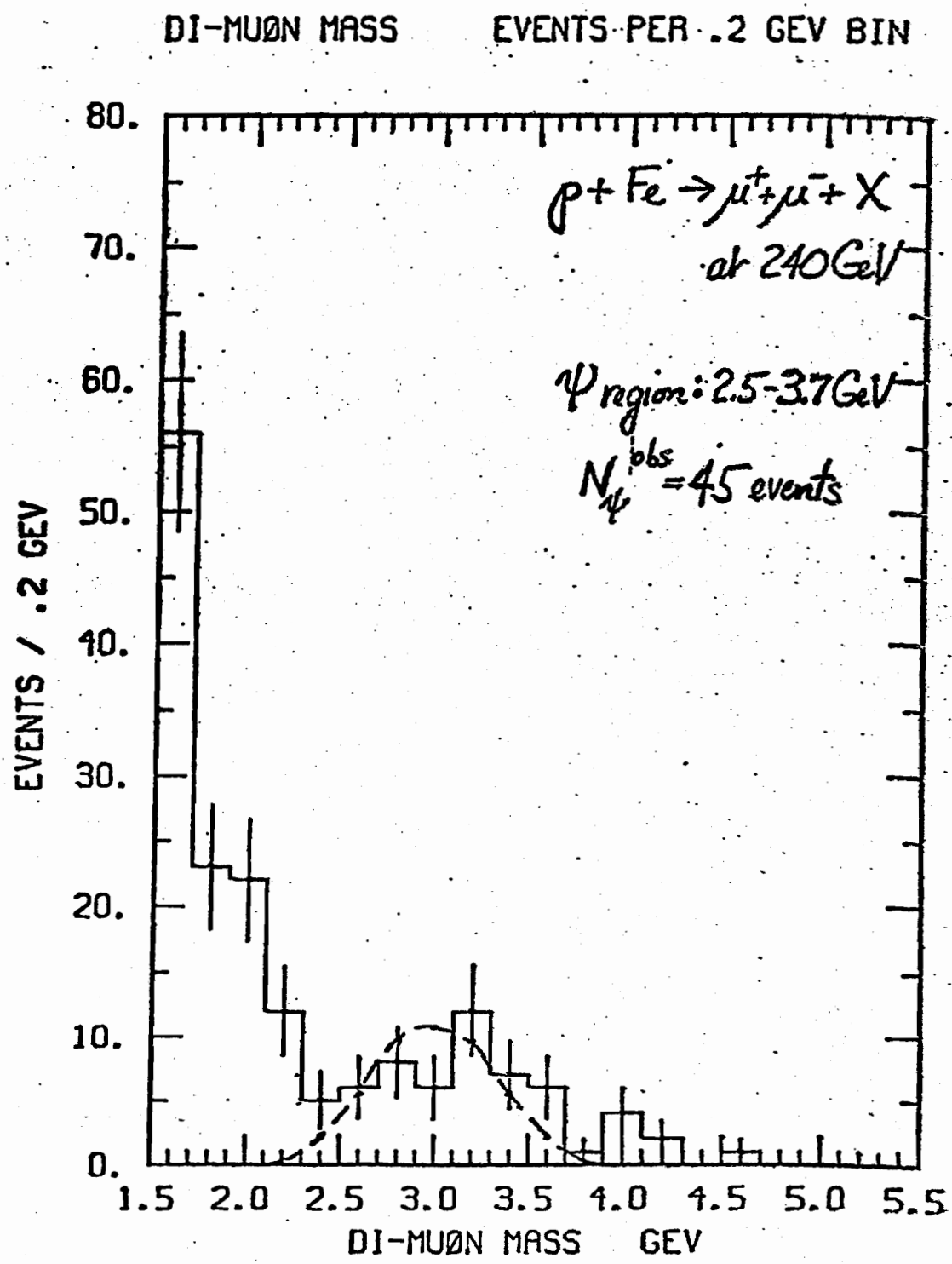
DI-MUØN MASS EVENTS PER .2 GEV BIN
p+Fe → μ⁺+μ⁻+X
at 240GeV
ψ region: 2.5-3.7GeV
N_ψ^obs = 45 events
EVENTS / .2 GEV
80.
70.
60.
50.
40.
30.
20.
10.
0.
1.5
2.0
2.5
3.0
3.5
4.0
4.5
5.0
5.5
DI-MUØN MASS GEV

Fig. 6

$2.5 < M_{\mu\mu} < 3.7$ GeV, the ψ region, result from the decay $\psi \rightarrow \mu^+\mu^-$. In the ψ region, we observe 104 and 45 events in the pion and proton data, respectively. Since the agreement between the dashed lines and the data is good, we interpret the observed enhancements as $\psi(3.1) \rightarrow \mu^+\mu^-$.

We have used the proportional chamber to check the source position for the events in the ψ region, $2.5 \leq M_{\mu\mu} \leq 3.7$ GeV. We consider only events which had a proportional chamber hit within 2 standard deviations of the calculated trajectory for each track. The proportional chamber hit and the position at the spark chambers were used to obtain a better measurement of the trajectory. The distribution of the z coordinate of the intercept in the horizontal plane of the two tracks is shown in Fig. 7. The resolution is poor but the mean is in good agreement with our assumed production point at z = 76 cm and the r.m.s. spread is in good agreement with Monte Carlo predictions.

We have chosen to present $X_L = P_{Lab}/P_{beam}$ and $P_\perp$ distributions corrected for the acceptance of the apparatus. To do this we wrote an event by event acceptance routine which assumes isotropic decay of the dimuon parent, neglects multiple scattering and uses a bend plane approximation to track through the magnet. To check this routine as well as to check all of our analysis routines we have generated Monte Carlo ψ events, let the muons multiple scatter and be accepted by a model of the apparatus, then corrected the events for acceptance. The resulting spectrum for a simulation of the X_L distribution for proton initiated ψ events, the distribution with the steepest slope, is shown in Fig. 8. There is reasonable good consistency; one can see the effect of the momentum resolution. We have checked that in all cases the disagreement between the best fit slope parameter and the generating parameter is less than the statistical errors for our measured slope parameters. Also, for the data, we have checked our

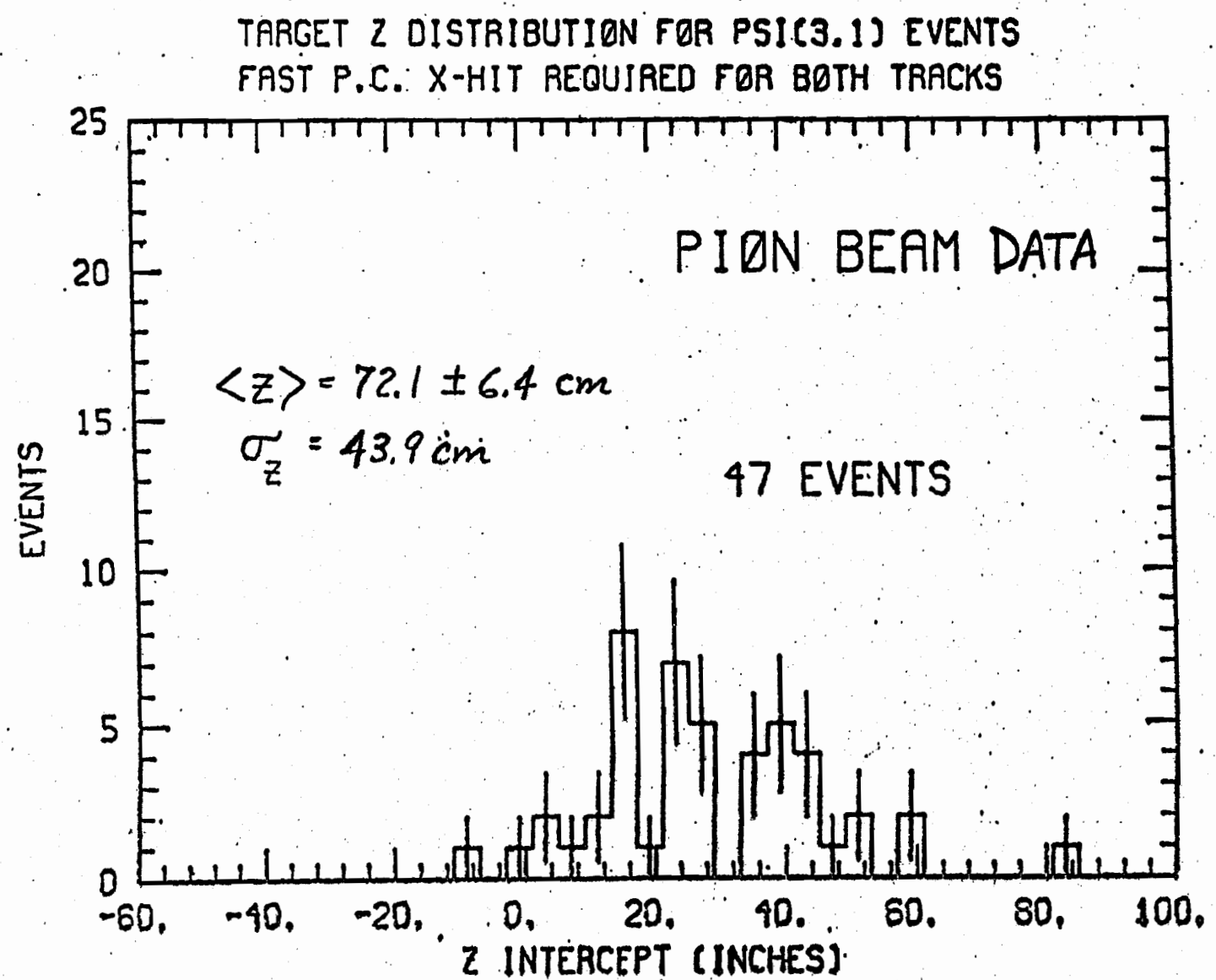
TARGET Z DISTRIBUTIØN FØR PSI(3.1) EVENTS
FAST P.C. X-HIT REQUIRED FØR BØTH TRACKS
PIØN BEAM DATA
<Z> = 72.1 ± 6.4 cm
σZ = 43.9 cm
47 EVENTS
EVENTS
0
5
10
15
20
25
-60.
-40.
-20.
0.
20.
40.
60.
80.
100.
Z INTERCEPT (INCHES)

Fig. 7

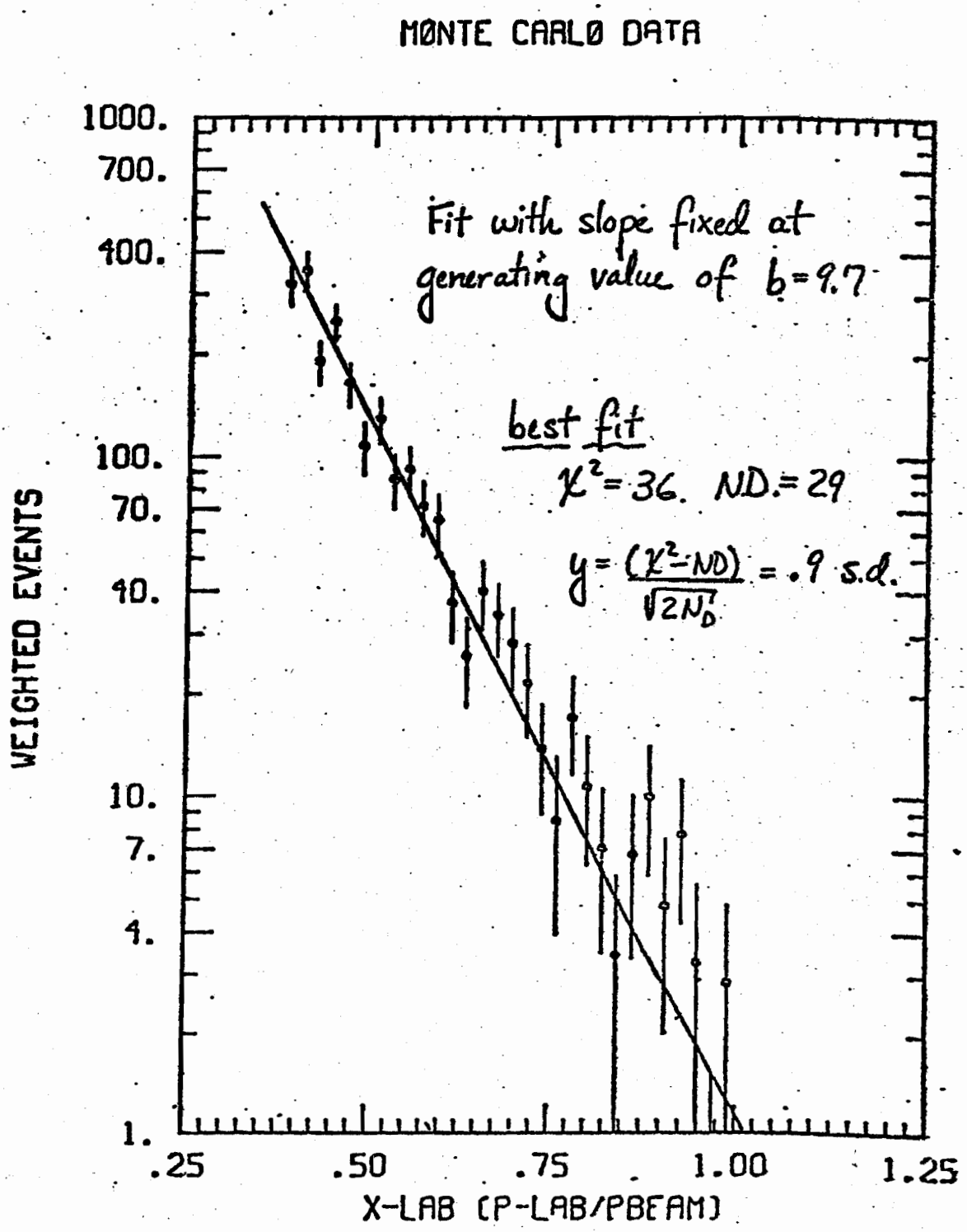
MØNTE CARLØ DATA
1000.
700.
400.
100.
70.
40.
10.
7.
4.
1.
WEIGHTED EVENTS
.25
.50
.75
1.00
1.25
X-LAB (P-LAB/PBEAM)
Fit with slope fixed at generating value of b=9.7
best fit
χ²=36. ND.=29
y=(χ²-ND)/√2N_D = .9 s.d.

Fig. 8

fitted slope parameters against paramaters obtained by fitting the uncorrected data directly using the Monte Carlo program.

The acceptance corrected distributions in X_L and $P_\perp$ for events in the ψ region are shown in Figs. 9 and 10. The solid lines are fits to the measured cross section of the form:

$$d^2\sigma/dX_L dP_\perp^2 \alpha \exp(-aX_L) \times \exp(-bP_\perp)$$

The results of the fits are for incidents pions $a_\pi = 6.2 \pm 0.8$ and $b_\pi = 1.6 \pm 0.2$ $(GeV)^{-1}$, and for incident protons $a_p = 9.7 \pm 1.6$ and $b_p = 2.2 \pm 0.5$ $(GeV)^{-1}$.

We have calculated using measured branching ratios of the $\psi'(3.7)$[3] that less than 7. $\pm$ 4.% of the yield in the ψ region, $2.5 \leq M_{\mu\mu} \leq 3.7$ GeV, is from $\psi'(3.7) \rightarrow \mu^+\mu^-$. From an extrapolation of a power law fit to the low mass data we find ~ 5% of the pion data and ~ 3% of the proton data in the ψ region is associated with the low mass region of our data, see Figs. 11 and 12. We are still analyzing the high mass data, $M_{\mu\mu} > 3.7$ GeV, and will try to understand the mass spectrum of events associated with these events and possible extrapolations into the ψ region. We calculate using π and γ inclusive spectra from πp and pp interactions, the measured ψ photoproduction cross section[4] and our own measured pion ψ production cross section and X_L distributions that the background in our pion and proton beam data due to secondaries is less than 6%. Using doubly charged data ($\mu^+\mu^+$ and $\mu^-\mu^-$), we find the background due to π and K decay is less than 2%. We are presently analyzing muon beam particle backgrounds but we believe this background to be negligible for the proton beam data and less than 10% for the pion beam data.

Using the MP counters, see Fig. 1, we have determined that our results are independent of whether or not we require a single minimum ionizing particle in the first counter. We chose not to cut on the

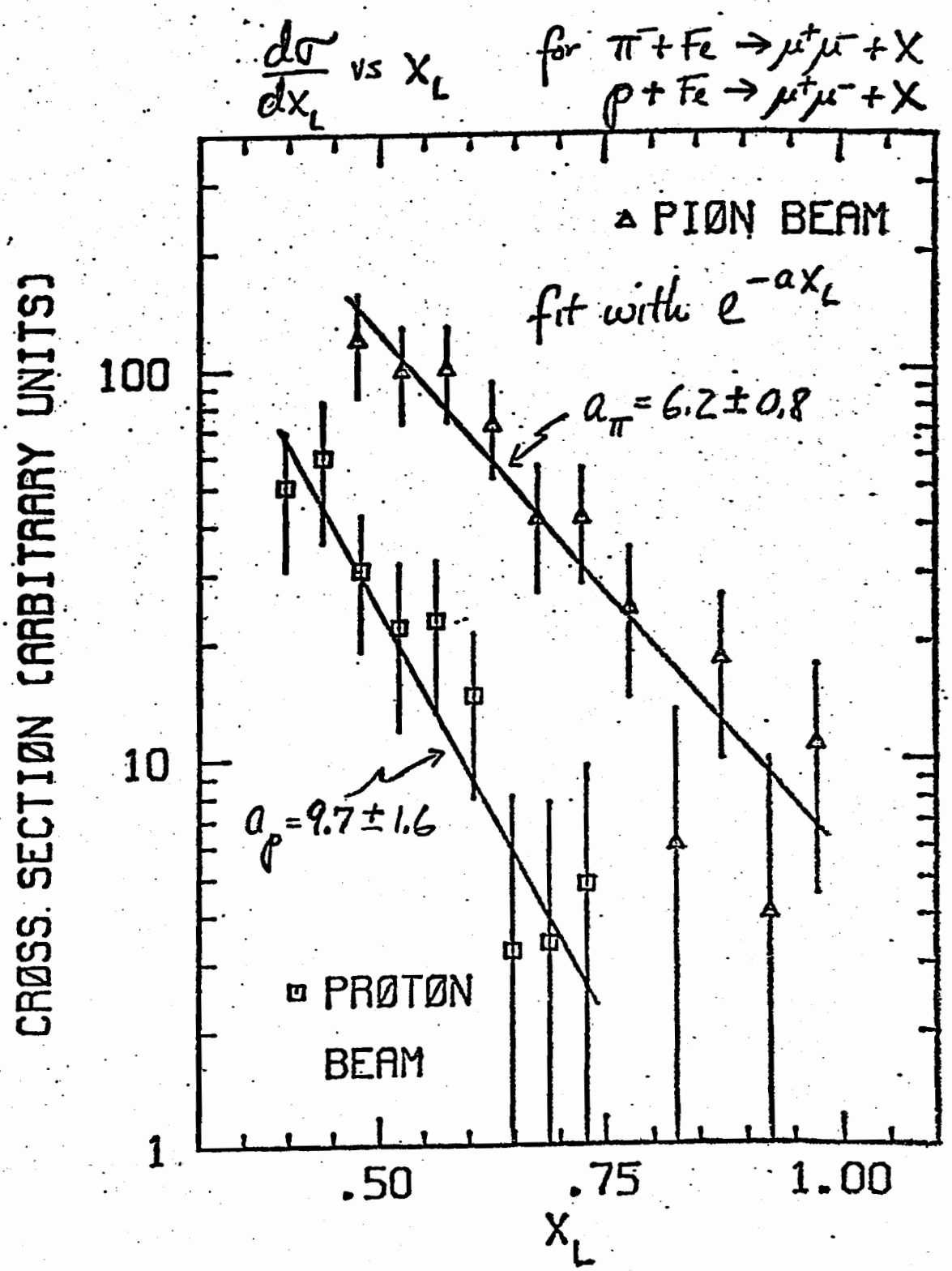
$\frac{d\sigma}{dx_L}$ vs X_L
for $\pi^- + Fe \to \mu^+\mu^- + X$
$p + Fe \to \mu^+\mu^- + X$
△ PIØN BEAM
fit with e^{-aX_L}
$a_\pi = 6.2 \pm 0.8$
$a_p = 9.7 \pm 1.6$
□ PRØTØN BEAM
CRØSS SECTIØN (ARBITRARY UNITS)
100
10
1
.50
.75
1.00
X_L

Fig. 9

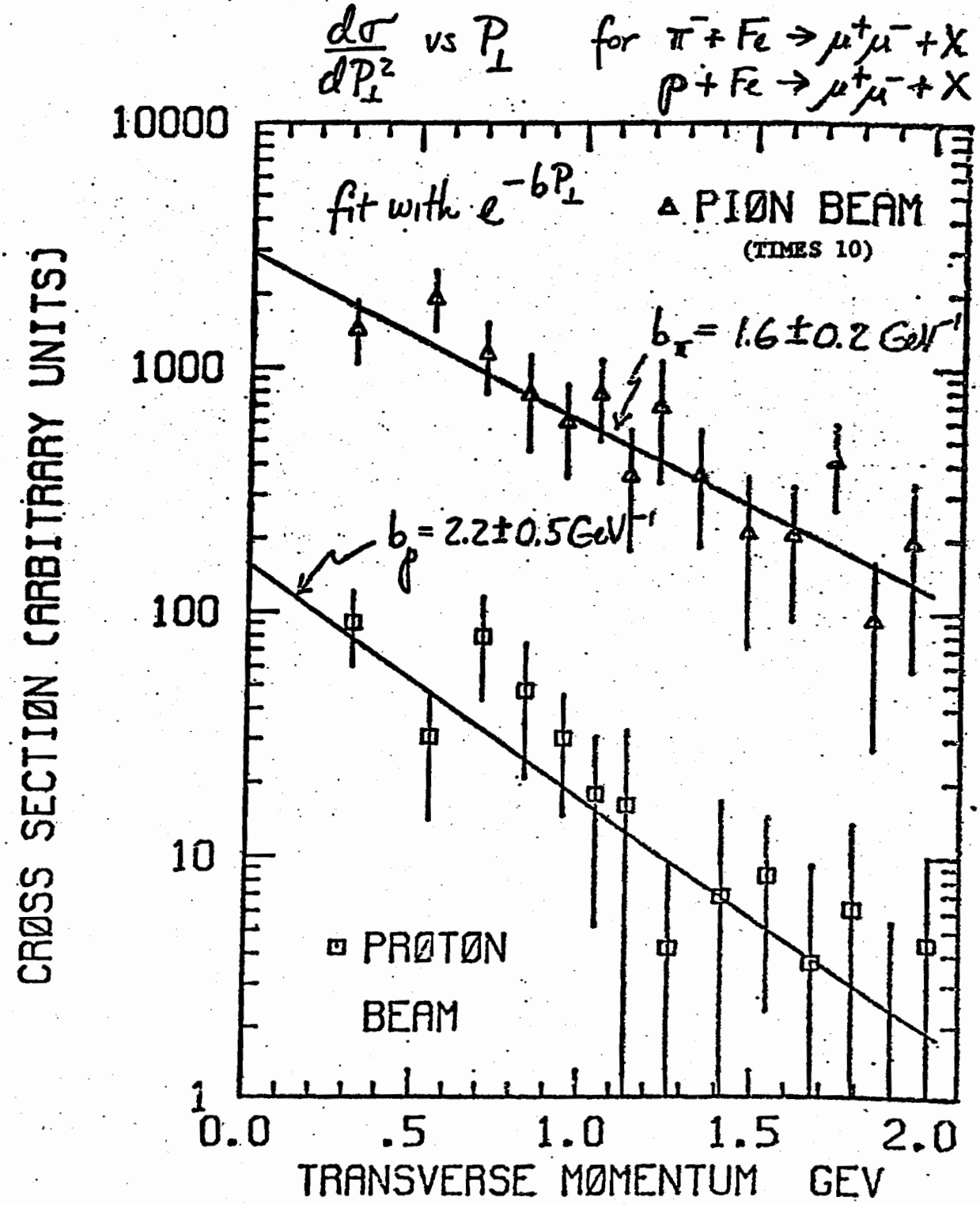
$\frac{d\sigma}{dP_\perp^2}$ vs $P_\perp$ for $\pi^- + Fe \to \mu^+\mu^- + X$
$p + Fe \to \mu^+\mu^- + X$
fit with $e^{-bP_\perp}$
PIØN BEAM
(TIMES 10)
$b_\pi = 1.6 \pm 0.2$ GeV^{-1}
$b_p = 2.2 \pm 0.5$ GeV^{-1}
PRØTØN
BEAM
CRØSS SECTIØN (ARBITRARY UNITS)
10000
1000
100
10
1
0.0
.5
1.0
1.5
2.0
TRANSVERSE MØMENTUM GEV

Fig. 10

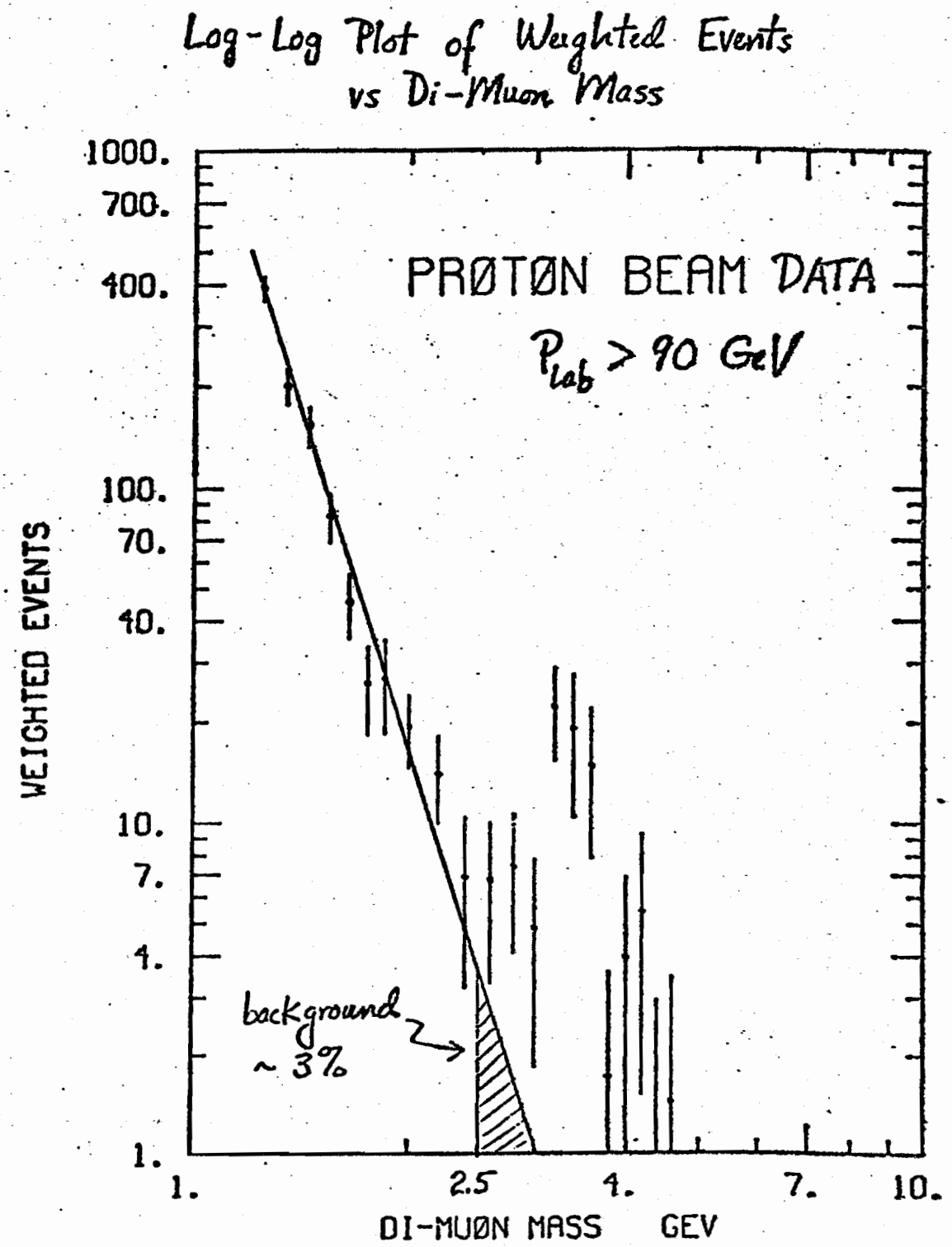
Log-Log Plot of Weighted Events
vs Di-Muon Mass
PRØTØN BEAM DATA
$P_{lab} > 90$ GeV
background
~ 3%
WEIGHTED EVENTS
1000.
700.
400.
100.
70.
40.
10.
7.
4.
1.
1.
2.5
4.
7.
10.
DI-MUØN MASS GEV

Fig. 11

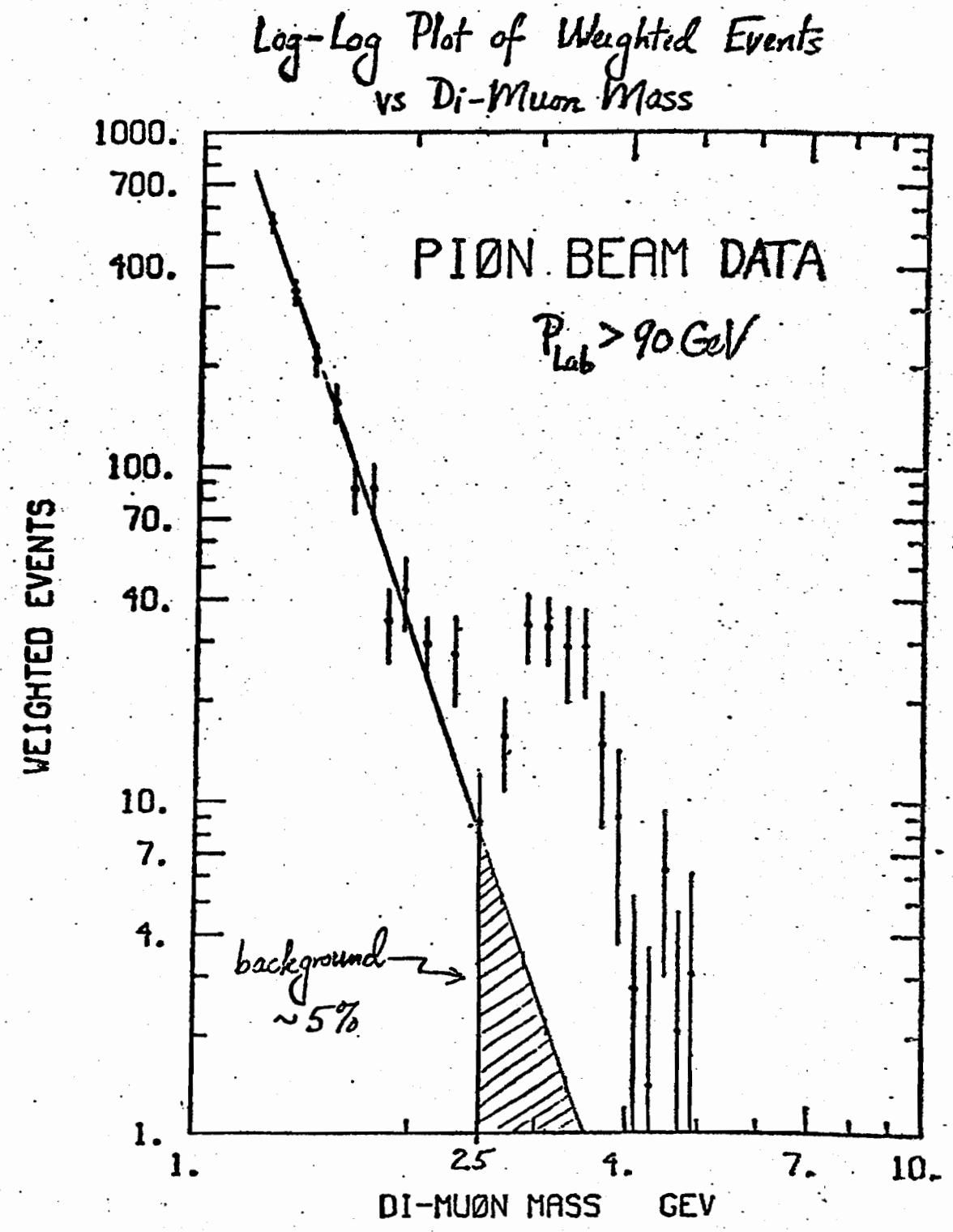
Log-Log Plot of Weighted Events
vs Di-Muon Mass
PIØN BEAM DATA
$P_{Lab} > 90$ GeV
WEIGHTED EVENTS
1000.
700.
400.
100.
70.
40.
10.
7.
4.
1.
background
~5%
1.
2.5
4.
7.
10.
DI-MUØN MASS GEV

Fig. 12

MP counters to avoid possible biases. We calculate that ~ 5% of our pion beam data and ~ 8% of our proton beam data may be associated with ψ production in the H_2 target.

We use the observed number of produced ψ's, corrections for detection efficiency, acceptance and target-X cut losses to calculate ψ production probabilities. At the present stage of analysis the backgrounds appear small. We have not done any background subtractions. We calculate the probability of producing a ψ per inelastic interaction in iron times the branching ratio into $\mu^+\mu^-$ to be:

$$P_\pi(\psi) = (1.58 \pm .79) \times 10^{-7},\ X' > .45$$

$$P_p(\psi) = (.59 \pm .30) \times 10^{-7},\ X' > .375$$

where the errors are an estimated $\pm$ 50% systematic error, and where we have used $X' \equiv X_L = P_{Lab}/P_{beam}$. We compare to the results of ψ production by neutrons on a Beryllium target[5] by calculating the implied production probabilities and comparing at the same X'_{min}, see Fig. 13. We find good agreement in slope but a factor of 4 discrepancy in normalization.

We have compared the yield of ψ mesons per incident π^-, Y_π, to the yield per incident p, Y_p. The ratio of the yields, $R = Y_\pi/Y_p$, is X'_{min} dependent. For $X' \geq .5$, $R = 7.4 \pm 2.0$, where the quoted error in R is dominated by the statistical uncertainty in Y_p. The fact that R is significantly greater than unity suggests that the mechanisms for ψ production at large X' are different for pions and protons. This difference may indicate that the antiquark in the π^- plays a critical role in ψ production.

For a total Fe inelastic cross section of ~ .7 barns our data gives for

$\pi^- Fe \rightarrow \psi \rightarrow \mu\mu$ $\sigma B = 109 \pm 55$ nanobarns for $X' > .45$

$pFe \rightarrow \psi \rightarrow \mu\mu$ $\sigma B = 41 \pm 21$ nanobarns for $X' > .375$

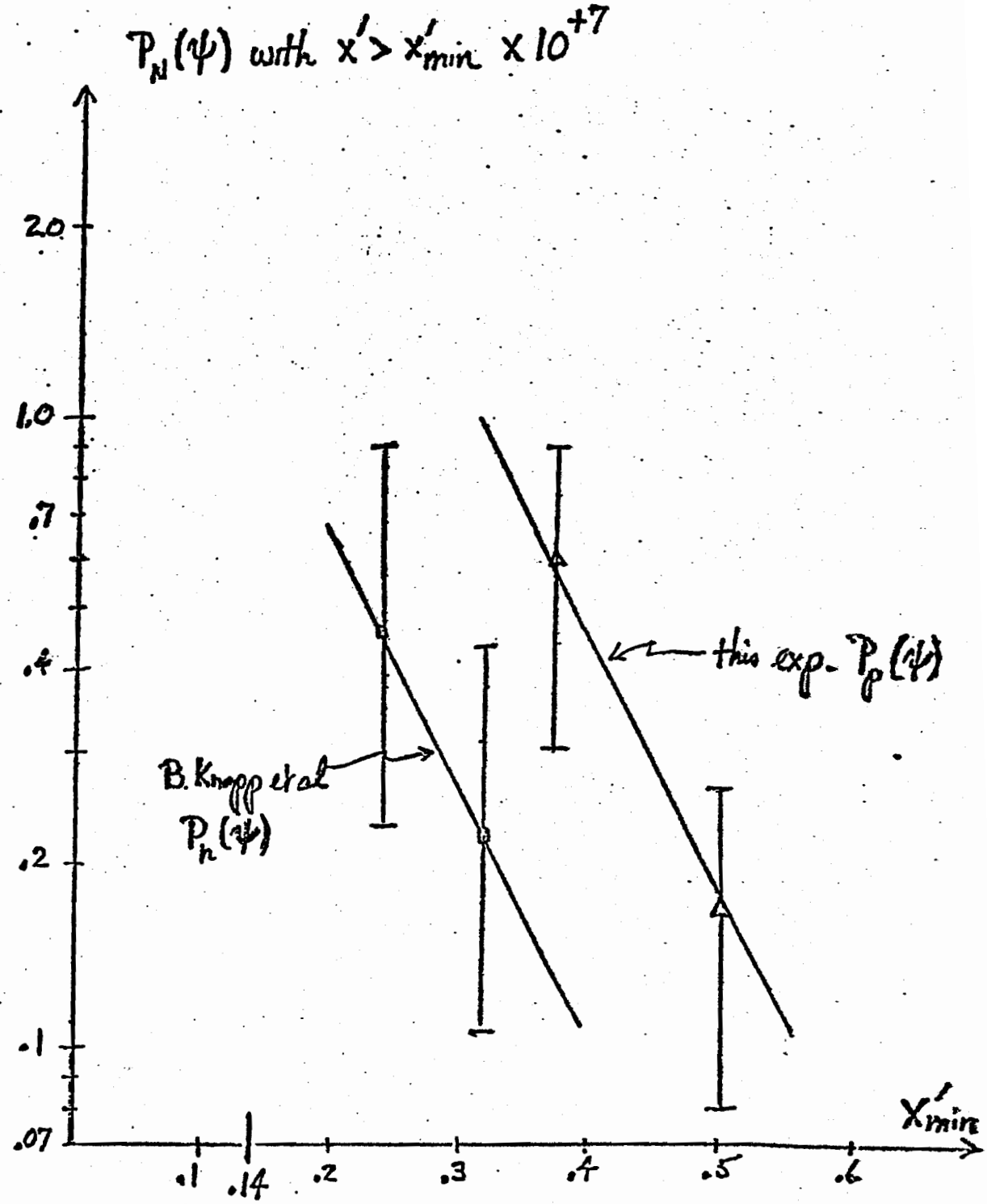
$P_N(\psi)$ with $x' > x'_{min}$ $\times 10^{+7}$
2.0
1.0
.7
.4
.2
.1
.07
.1
.14
.2
.3
.4
.5
.6
x'_{min}
this exp. $P_p(\psi)$
B. Knapp et al
$P_n(\psi)$

Fig. 13

Using inelastic cross sections of 32 mb for pp and 21 mb for πp, neglecting absorption of the ψ in the Fe nucleus ($\approx$ 5% effect) and using the branching ratio of ψ into $\mu\mu$[3] we find

$$\sigma_{\pi N}(\psi) \simeq 48 \pm 24 \text{ nanobarns/nucleon, } X' > .45$$

$$\sigma_{pN}(\psi) \simeq 27 \pm 14 \quad \text{"} \quad \text{"} \quad X' > .375$$

Extrapolating to X' = .14, assuming no break in slope, multiplying by 2 for production in the forward and backward hemisphere, we estimate that the total ψ production cross section in proton nucleon collisions is $\approx .54 \pm .36$ microbarns.

In Figs. 14 and 15 I show the dimuon effective mass spectra for all events, which satisfy the criteria discussed earlier, for the pion and proton beam runs. These data are not corrected for variation of spectrometer acceptance with mass. I would like to point out only a few features of the low mass, $M_{\mu\mu} < 2.5$ GeV, region of our data since we are still analyzing them. First, there is a general similarity in shape of the two mass spectra and an overall factor of $\sim$ 2.5 higher yield by pions compared to the yield by protons even though the data is cut at a higher X' for the pion beam data than for the proton beam data (X'_{min} is .45 for the pion beam data and .375 for the proton). Secondly, there is a peak in the mass spectrum at $\approx$ 700 MeV which may or may not be entirely inclusive ρ^o production.

We have corrected the data for acceptance in the region $1.2 \leq M_{\mu\mu} \leq 2.5$ GeV, see Figs. 11 and 12 and have found a M^{-n} dependence with $n \approx 6$ for both the pion and proton beam data. We have also compared the yield per incident pion to that per incident proton above the same X'_{min}. We find for X' > .5, $R(\pi/p) \simeq 4.7$ compared to $R(\pi/p) = 7.4 \pm 2.0$ for the ψ region. These facts may suggest that dimuons in the $1.2 \leq M_{\mu\mu} \leq 2.5$ GeV mass region are produced by the same process by which ψ's are produced and that the basic interactions by

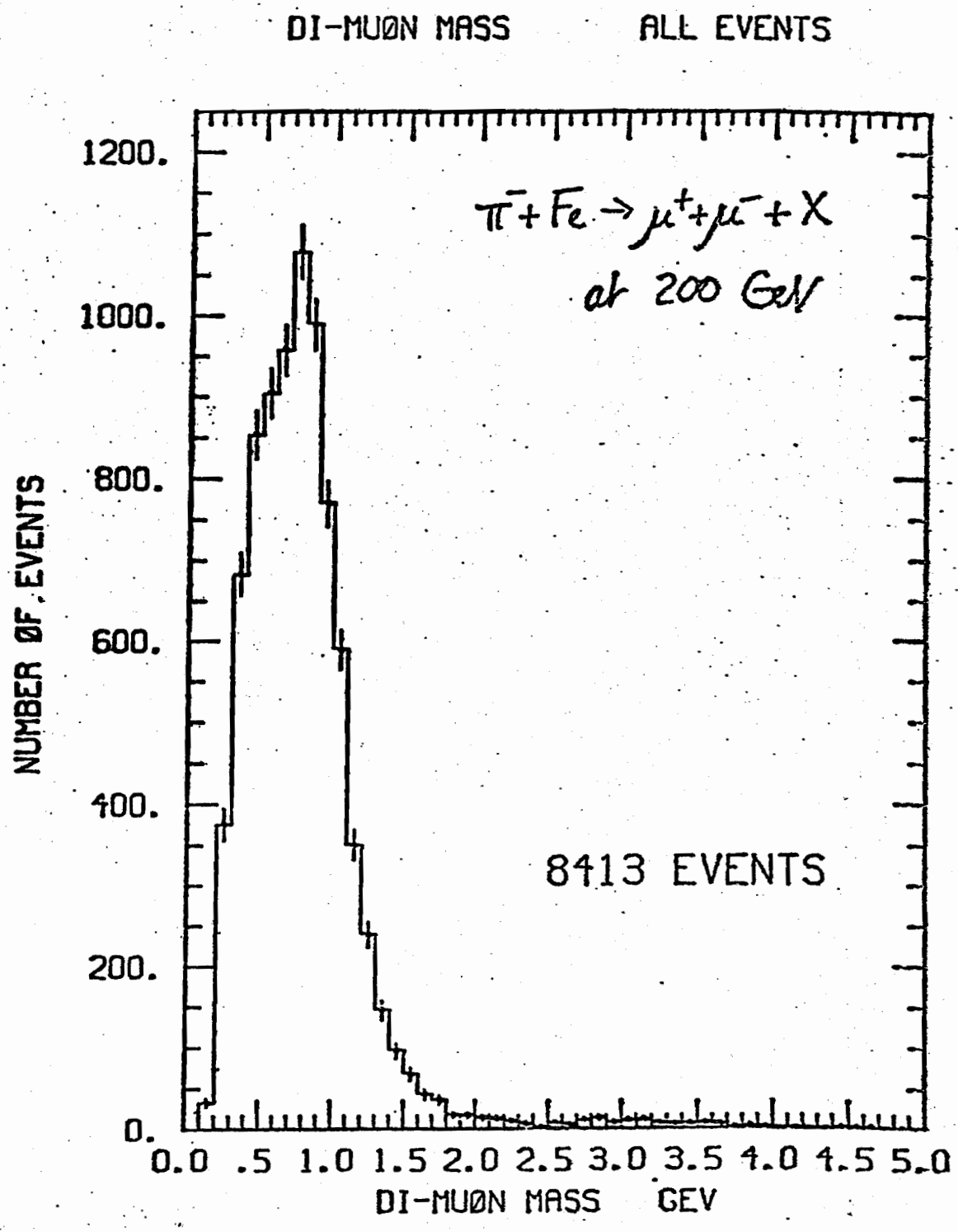
DI-MUØN MASS ALL EVENTS
$\pi^- + Fe \rightarrow \mu^+ + \mu^- + X$
at 200 GeV
8413 EVENTS
NUMBER ØF EVENTS
1200.
1000.
800.
600.
400.
200.
0.
0.0 .5 1.0 1.5 2.0 2.5 3.0 3.5 4.0 4.5 5.0
DI-MUØN MASS GEV

Fig. 14

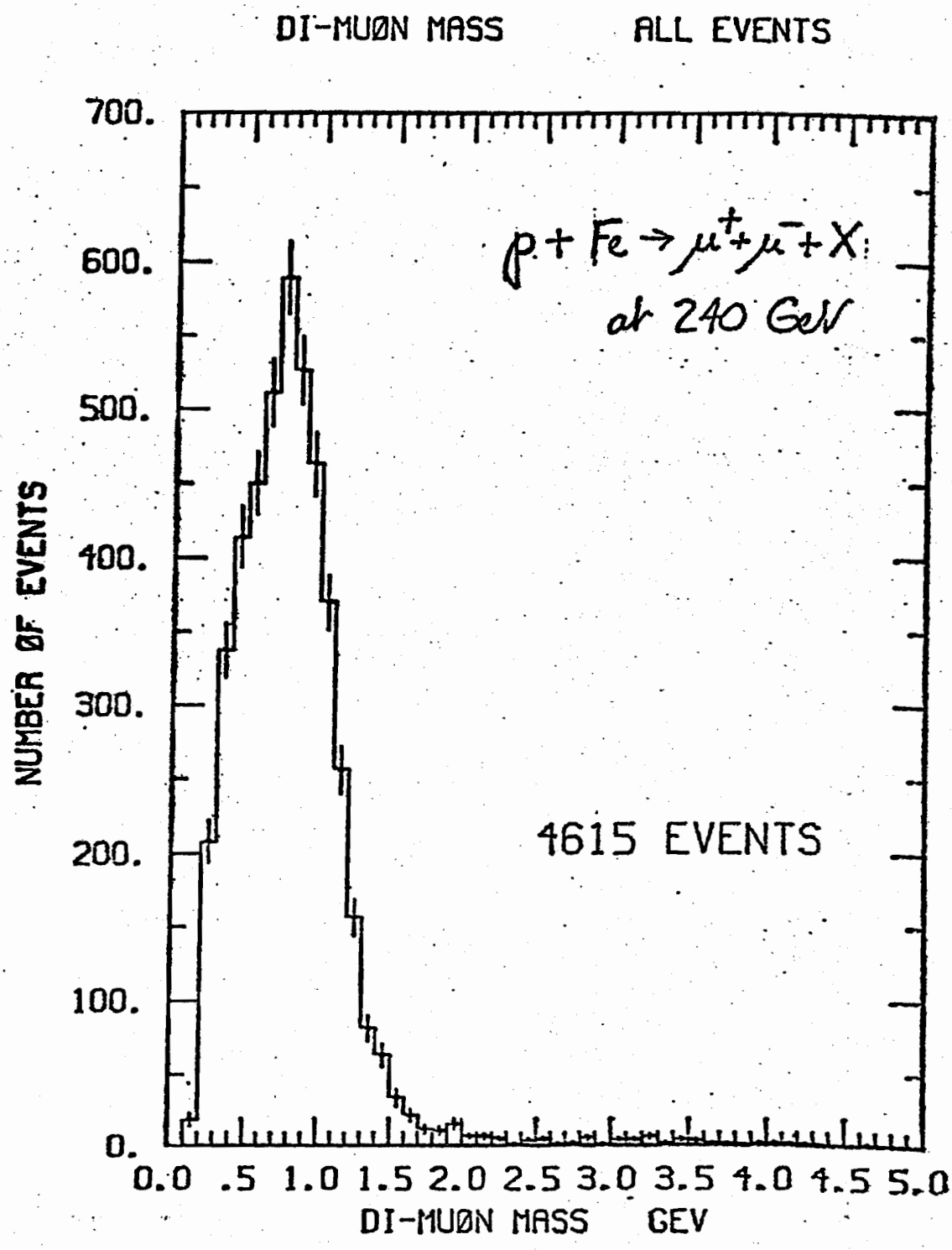
DI-MUØN MASS ALL EVENTS
700.
600.
500.
400.
300.
200.
100.
0.
NUMBER ØF EVENTS
p + Fe → μ+ + μ− + X
at 240 GeV
4615 EVENTS
0.0 .5 1.0 1.5 2.0 2.5 3.0 3.5 4.0 4.5 5.0
DI-MUØN MASS GEV

Fig. 15

which pions and protons produce dimuons are similar but differ in strength. Finally, I would like to remind you that we are still analyzing the low mass region and have not completely understood apparatus effects in the measurement of these data in that region.

REFERENCES

1. J. J. Aubert, et al., Phys. Rev. Lett. 33, 1404 (1975) and J. E. Augustin, et al., Phys. Rev. Lett. 33, 1406 (1975).

2. This report gives in more detail results previously reported, G. Blanar, et al., Phys. Rev. Lett. 35, 346 (1975).

3. A. M. Boyarski, et al., Phys. Rev. Lett. 34, 1357 (1975) and J. A. Kadyk, et al., LBL report #3687 (unpublished).

4. B. Knapp, et al., Phys. Rev. Lett. 34, 1040 (1975).

5. B. Knapp, et al., Phys. Rev. Lett. 34, 1044 (1975).